

UCLA

UCLA Electronic Theses and Dissertations

Title

Cellular adaptations in the crista epithelia of the Egyptian fruit bat

Permalink

<https://escholarship.org/uc/item/3z6745s4>

Author

Ton, Ymi

Publication Date

2017

Peer reviewed|Thesis/dissertation

UNIVERSITY OF CALIFORNIA

Los Angeles

Cellular adaptations in the crista epithelia
of the Egyptian fruit bat

A thesis submitted in partial satisfaction
of the requirements for the degree Master of Science
in Physiological Science

by

Ymi Ton

2017

© Copyright by

Ymi Ton

2017

ABSTRACT OF THE THESIS

Cellular adaptations in the crista epithelia
of the Egyptian fruit bat

by

Ymi Ton

Master of Science in Physiological Science
University of California, Los Angeles, 2017
Professor Walter Helmut Metzner, Chair

We believe that the flight and echolocation behaviors displayed by the Egyptian fruit bat (*Rousettus aegyptiacus*) may translate to more precise head movement coding in response to their unique sensorimotor demands. While there is evidence for a relationship between locomotive behaviors and structural adaptations in the bony labyrinth of birds and mammals, none exist in the bat's bony labyrinth. The present study determines whether cellular adaptations that translate to increased capability for high fidelity head movement coding exist in the crista central zone of *Rousettus*. This was accomplished using immunohistochemical techniques comparing hair cell and afferent phenotypes within crista central zone of *Rousettus* and the mouse (*Mus musculus*). Central zone hair cell counts revealed an increased fraction of type I hair cells in *Rousettus*. Additionally, *Rousettus* exhibits increases in the proportion of higher

order complex calyces within the central zone. The calcium binding protein OCM is also observed to have expression that is restricted to type I hair cells in the central zone of *Rousettus*, unlike in *Mus* where it is also expressed in type II hair cells. KCNQ4, a low-voltage activated potassium channel, exhibits a positive association with CALB2 expression in the central zone of both *Rousettus* and *Mus*, which suggests that their association may contribute to the unique response characteristics of calyx-only afferents that project to the central zone. These findings provide evidence that the crista epithelia of *Rousettus* exhibits cellular adaptations that are consistent with enhanced head movement coding that may serve to be advantageous to their unique behavioral niche.

The thesis of Ymi Ton is approved.

Peter M. Narins

Felix Erich Schweizer

Larry F. Hoffman

Walter Helmut Metzner, Committee Chair

University of California, Los Angeles

2017

TABLE OF CONTENTS

Abstract	ii
Acknowledgments	vii
Introduction	1
Methods	4
Results	17
Discussion	26
Figures	32
Tables	37
Appendix: Supplemental Figures	39
References	42

LIST OF TABLES AND FIGURES

Figure 1	32
Figure 2	33
Figure 3	34
Figure 4	35
Figure 5	36
Table 1	37
Table 2	37
Table 3	38
Table 4	38
Supplemental Figure 1	39
Supplemental Figure 2	40
Supplemental Figure 3	41

ACKNOWLEDGMENTS

Thank you to my patient and invested mentors as well as committee members for all of their input and guidance. Lastly, thank you to my family and peers for their support during this endeavor.

INTRODUCTION

The Egyptian fruit bat (*Rousettus aegyptiacus*) utilizes wing beat frequencies between 6-8 Hz (Riskin et al. 2010) which are reflective of similar frequencies in their body movement and likely head movement. *Rousettus aegyptiacus* and other members of this genus are particularly unique among megabats because they rely on echolocation, in addition to vision, to navigate their environment and to locate targets while in flight (Möhres and Kulzer 1956; Yovel et al. 2010). Previous studies have revealed that the bats' vestibular system, calibrated by echolocation and visual cues, is important for their flight control and orientation (Horowitz, Cheney and Simmons 2004). Some studies have sought to identify structural adaptations within the bats' bony labyrinth that may be associated with their unique behavioral niche since a relationship between locomotive behaviors and structural adaptations of in birds (Hadziselimmovic and Savkovic 1964) and in mammals (Spoor et al. 2007; Malinzak, Kay and Hullar 2012) bony labyrinths has been demonstrated. However, although some bats have enlarged cochleae in response to echolocation, structural adaptations in their bony labyrinth do not exist (Ramprashad et al. 1980; Davies et al. 2013). This raises the question of where within the bats' vestibular system these sensory adaptations exist. This study addresses this question by examining cellular adaptations present in the cristae ampullares, the inner ear head rotational receptors, that may serve to accommodate the sensorimotor demands experienced by *Rousettus*.

The crista can be divided into separate regions distinguished by their unique morphological and physiological characteristics. Previously, the crista was divided into three regions of approximately equal area based on hair cell density: the innermost central zone, the intermediate zone, and the outermost peripheral zone (Lindeman 1969; Fernández, Lysakowski and Goldberg 1995). Lysakowski and Goldberg (1997) have since suggested that these three

regions are insufficient in explaining the regional variations in the cellular and afferent architecture of the crista.

The regions of the crista have since been redefined to simply the central and peripheral zones, and is the definition utilized by this study. The redefined central zone is the innermost region of the crista that encompasses calyx-only afferents (afferents with strictly calyceal endings), while the outermost peripheral zone is absent of this special class of afferents (Desai, Ali and Lysakowski 2005). The calyx-only afferents can be distinguished from other vestibular afferents because they are the only class of afferents that are calretinin (CALB2) immunoreactive (Desmadryl and Dechesne 1992). In addition to the calyx-only afferents, two other classes of afferents innervate the crista epithelia and can also be distinguished by their dendritic arborization (Fernández, Baird and Goldberg 1988). Dimorphic afferents, found in both the central and peripheral zones, have calyceal and bouton endings. Both calyx-only and dimorphic afferents can be further categorized as simple or complex calyces if associated with one or two or more calyces, respectively. Lastly, bouton-only afferents are found only in the peripheral zone and have strictly bouton endings. Special classes of sensory hair cells are also found distributed throughout the sensory epithelia. Type I hair cells are characterized by their innervation by calyceal endings, while type II hair cells are innervated by bouton endings (Engstrom 1961). Type I hair cells can be further divided into two subtypes: type Ic hair cells that contact calyx-only afferents, and type Id hair cells that contact dimorphic afferents (Li, Xue and Peterson 2008).

In mammals, the afferents projecting from the two regions of the crista have different activity. The calyx-only and dimorphic afferents projecting from the central zone exhibit phasic, irregularly discharging, and higher sensitivity in response to head rotations, while those

dimorphic and bouton-only afferents projecting from the peripheral zone display tonic and regularly discharging responses (Baird et al. 1988; Goldberg et al. 1990; Hullar and Minor 1999, Sadeghi et al. 2007; Yang and Hullar 2007; Lasker et al. 2008). Early in our investigation, we observed that the calcium binding protein oncomodulin (OCM) that is distributed throughout the cytoplasm of a subset of vestibular hair cells (Simmons et al. 2010) has enhanced immunoreactivity in the central zone compared to the peripheral zone. Similar to OCM, the low-voltage activated potassium channel KCNQ4, located in the calyx inner face, has also been shown to have enhanced immunoreactivity in the central zone (Lysakowski et al. 2011; Spitzmaul et al. 2013). Altogether, the enhanced expression of OCM and KCNQ4 in conjunction with the distribution of hair cells and afferents that are more sensitive to head rotation found in the central zone make it a candidate region of the crista epithelia to explore cellular adaptations in mammals with unique agile behaviors, such as *Rousettus*.

Through a comparative analysis of *Rousettus* and the mouse (*Mus musculus*), we test hypotheses that cellular markers important for head movement coding found in the crista central zone have similar distributions in *Rousettus* and *Mus*. Rejection of these hypotheses will provide valuable insight into cellular adaptations developed by *Rousettus* that may be advantageous to their flight and echolocation behaviors.

METHODS

Animals and harvesting of crista epithelia

All procedures were approved by the Chancellor's Animal Research Committee. Adult male and female *Rousettus* animals and adult male C57Bl/6 mice (5-6 weeks old) were used in this study.

To harvest the crista epithelia, animals were deeply anesthetized using either intraperitoneal injection of sodium pentobarbital (80mg/kg, *Rousettus*) or exposed to isoflurane (*Mus*). After decapitation, the vestibular epithelia were immediately fixed with 4% paraformaldehyde in 0.1 M phosphate buffer, pH = 7.4, either through the oval window (*Rousettus*), or through a fenestra created in the caudomedial temporal bone (*Mus*). Both temporal bones were rapidly harvested from each animal and then immediately immersed and left in fixative overnight (*Rousettus*) or for 3 hours (*Mus*). After proper fixation, the cristae were micro-dissected from the temporal bones with the nerves closely trimmed and thoroughly rinsed with 0.1 M phosphate buffer saline (PBS). The cristae were stored in 0.1 M PBS until ready to be further processed with thermolysin.

Thermolysin application

Incubating the cristae in a solution containing thermolysin (a heat-activated protease; Sigma, P1512) that breaks down the underlying stroma served two purposes for our study. First, it enabled better penetration of the antibodies used in the subsequent immunohistochemical experiments. Second, it helped flatten the three-dimensional saddle shape of the tissue by enabling us to micro-dissect the sensory epithelia from the underlying stroma. Thus, the treatment of the cristae with a thermolysin solution resulted in better immunolabelling and easier

whole mount preparation of the cristae for confocal microscopy imaging and analysis. Modifications were made to the thermolysin procedure for flattening fixed crista previously outlined by Desai et al. (2005) for application on both *Rousettus* and *Mus* cristae used in our study. Incubating the cristae in a thermolysin solution (1 µg/50 ml thermolysin, 2 mM Tris, 1mM CaCl₂) while in a 55°C water bath yielded the best preparation of the cristae without compromising the integrity of the epithelia. Optimal incubation times varied between the two species, with the *Rousettus* requiring 4 hours and the *Mus* requiring 2.5 hours incubation time. After incubation in the thermolysin solution, the cristae were thoroughly rinsed of the thermolysin solution with 0.1 M PBS (5 X 10 min).

Immunohistochemistry

Immunohistochemistry was performed on the thermolysin-treated cristae to identify various hair cell and afferent phenotypes distributed throughout the sensory epithelia. The cristae were first incubated in blocking solution (1% Triton X-100, 10% 10x fish gelatin blocking buffer, in 0.1 M PBS) for 2 hours at room temperature. After completion of the blocking procedure, the cristae were then incubated in a primary antibody solution prepared in blocking solution uniquely prepared for each analysis. All primary antibody solutions contained primary antibodies against CALB2 and neuronal class III β-tubulin (TUBB3). The primary antibody against CALB2 was used to delineate the central zone in the cristae, to identify calyx-only afferents, and to obtain counts of central zone type Ic hair cells. The primary antibody against TUBB3 was used to identify all calyces of the sensory epithelia, and to obtain counts of central zone type I hair cells. Primary antibodies against either OCM or KCNQ4 were also included in the primary antibody solution as dependent on the analysis.

After incubation in the primary antibody solution for 72 hours at 4°C, the cristae were rinsed well of the primary antibody solution with 0.1 M PBS (3 X 10 min.), then left to incubate in a secondary antibody and stain solution prepared in 0.1 M PBS at room temperature for 2 hours. Fluorophore-conjugated phalloidin (PHAL), which labels the filamentous actin of the stereocilia bundles located on the apical surface of the hair cells, was included in all secondary antibody and stain solutions in order to obtain counts of all central zone hair cells. After incubation in the secondary antibody and stain solution, the cristae were rinsed well using 0.1 M PBS (3 X 10 min.) and left in 0.1 M PBS until ready to be mounted. Information regarding specific primary and secondary antibody solutions are included in Table 1.

Antibody specificity

For the OCM and KCNQ4 expression analyses, no primary antibody OCM and KCNQ4 control specimens were immunoprocessed in parallel (same day and batch processing, identical confocal imaging parameters) with positive immunolabelled specimens to examine non-specific binding of fluorophore conjugated secondary antibodies and background fluorescence without the presence of the primary antibody under evaluation. For each animal, no primary control specimens were obtained from the contralateral ear and immunoprocessed without the primary antibody against OCM or KCNQ4.

Confocal microscopy

The immunolabelled cristae were mounted on Superfrost Plus Microscope Slides (12-550-15, Fisher Scientific) with a Secure-Seal Spacer (9 mm diameter, 0.12 mm deep, S24737, Fisher Scientific). Cristae were immersed in EverBrite mounting medium (23001, Biotium) and

covered with number 1.5 coverslips (18x19 mm, 12-541A, Fisher). Confocal images of whole-mounted cristae were captured with either an upright Zeiss LSM 710 or 880 confocal microscope using the ZEN Black confocal microscopy program. Using the Zeiss LSM 880 confocal microscope, imaging parameters (e.g. laser intensities, gains) were carefully matched between experimental and their paired no primary control specimens. The 405 nm (0-2%), 488 nm (0-0.5% intensity), 561 nm (0-0.25% intensity) and 633 nm (0-2.5% intensity) laser lines were used for excitation. A Zeiss Plan-Neofluar 20X/0.8 objective was used to capture low magnification, tiled image stacks, while a Zeiss Plan-Apochromat 63X/1.4 NA oil-immersion objective was used to capture high magnification image stacks. For all collected confocal images, the overall x-y scan size was 1024 x 1024 pixels, with the total stack depth dependent upon epithelial region and the degree by which the crista laid flat on the microscope slide. The optical section thickness for all collected images was 0.37 μm . Sufficient optical sections were collected for each specimen to include complete visualization starting from the apical surface of the sensory epithelia, including the hair cell stereocilia, basally to the support cell layer. Confocal images of the whole-mount immunolabelled cristae were collected such that the entire central zone for each specimen was acquired along with at least two regions from the planum semilunatum located directly outside of the central zone. Low power images were acquired at 1.4x zoom for *Rousettus* and 1.5x zoom in *Mus*, while high power images were acquired at 1.0x zoom for both species. All confocal images collected for this study were either of 8 or 12-bit depth. Sum slices projections, a single output image that is the sum of the slices (sum of all pixels for each location) in a stack, were prepared using *FIJI* image analysis software. Scale bars were placed on confocal images by calculating $\mu\text{m}/\text{pixel}$ ratios.

Quantification of central zone hair cells and calyces

High magnification confocal images of the immunolabelled cristae were imported into *Neuroleucida* (version 6.02.2) for central zone hair cell and calyx quantification. Individual channels were separated from multi-channel high power confocal image stacks to create single channel stacks that were imported into *Neuroleucida*. Single channel stacks were stitched together to produce a carefully reconstructed confocal stack of each crista with complete visualization of the central zone in each channel to prevent double counting of hair cells and calyces. Using the stitched stacks with the single channel representative of CALB2 immunolabelling, the central zone was demarcated by tracing a contour around the region of the sensory epithelium containing CALB2 immunolabelled calyces. After identifying the central zone, hair cells within the traced contour were quantified. To obtain counts of total hair cells, all hair cells were identified by their PHAL-stained base of the stereocilia and kinocilium (that is not stained with PHAL) using the single channel representative of PHAL staining. Total type I hair cell counts were obtained by identifying all calyces (which encompass type I hair cells) using the single channel representative of TUBB3 labelling. Total type Ic hair cells counts were obtained by identifying all CALB2 immunolabelled calyces (which encompass type Ic hair cells) using the single channel representative of CALB2 labelling. Total type II hair cell counts were deduced by subtracting the total number of type I hair cells from the total number of hair cells counted. Similarly, total type Id hair cell counts were deduced by subtracting the total number of type Ic hair cells from the total number type I hair cells counted.

Central zone calyces associated with either simple or complex calyces were also quantified. Simple and complex calyces were distinguished by navigating the reconstructed high power confocal stacks of each crista along its apical-basal axis and identifying the number of

calyces associated with a single parent axon within the contoured central zone. Simple calyces were identified as those associated with one calyx, whereas complex calyces were identified as those associated with two or more calyces. Among the complex calyces, those associated with two calyces (doublets), three calyces (triplets), four calyces (quadruplets), and five calyces (quintuplets) were also identified.

OCM expression analysis

Initial qualitative observations of confocal images suggested heterogeneous expression of OCM among central zone hair cells in both *Rousettus* and *Mus*. To define the level of emission intensity that would be considered positive OCM expression within central zone hair cells in both *Rousettus* and *Mus*, all positively immunolabelled cristae used for this analysis were compared to a paired no primary control specimen obtained from the contralateral ear in order to accommodate any variation in fixation, immunohistochemical processing, and imaging parameters among specimens. Effectively, any OCM emission intensities measured from central zone hair cells in the no primary control specimens would be the result of background emission caused by non-specific binding of the fluorophore conjugated secondary antibody or background fluorescence. Therefore, if any central zone hair cell from the experimental specimens displayed a greater emission intensity than that of the paired no primary control specimen, we would conclude that it was the result of the presence of the primary antibody against OCM. We defined the threshold that would be considered OCM positive expression individually for each experimental specimen. This threshold was defined as the mean plus 4 standard deviations of mean emission intensities measured from a sample of central zone hair cells in its matched no primary control specimen. Using this metric, assuming that the mean OCM emission intensities

among central zone hair cells of no primary control specimens are normally distributed, any central zone hair cell from the experimental specimens with a mean emission intensity greater than the determined threshold was considered to have probability of $P < 10^{-4}$ of being OCM negative, or having an emission intensity comparable to the population of central zone hair cells of the no primary control specimen.

However, upon use of this threshold established by the no primary control specimens, we discovered that all hair cells measured from experimental *Rousettus* and *Mus* specimens, including hair cells in the central zone as well as those sampled from the planar region, displayed mean emission intensities well above this threshold. Examples of OCM emission of central zone hair cells in a no primary control *Rousettus* specimen and of planar region hair cells of a positively immunolabelled *Rousettus* specimen are shown in Supplemental Fig. 1. This finding suggests that all hair cells, including planar region hair cells, in both *Rousettus* and *Mus* display some basal level of OCM emission.

Since we want to focus on enhanced OCM emission within the central zone, we altered our criteria such that each experimental specimen served as its own internal control. We defined the new threshold emission intensity that would be considered OCM positive expression individually in each experimental specimen. This new threshold was defined as the mean plus 4 standard deviations of the mean emission intensities measured from a sample of hair cells located in its planar region. Using this metric, assuming that the mean OCM emission intensities among planar region hair cells are normally distributed, any central zone hair cell with a mean level of emission intensity greater than the newly determined threshold was considered to have a probability of $P < 10^{-4}$ of being OCM negative, or having an emission intensity comparable to the population of planar hair cells.

OCM emission among central zone hair cells was evaluated using the image processing program *FIJI*. High power 12-bit confocal images of the cristae immunolabelled with PHAL, CALB2, OCM, and TUBB3 were imported into *FIJI* and the central zone within each confocal stack delineated by identifying the region encompassing CALB2 labelled calyces. To extract OCM emission intensities, a uniform circle with a radius of 20 pixels (equivalent to 2.635 microns) was traced and placed in the center of each central zone hair cell within a single carefully chosen optical section of the confocal stack under the single channel representative of OCM labelling. For each type I hair cell, OCM emission intensity measurements were obtained from the optical section along the principal axis of the hair cell where the innervating calyx had the largest circumference. For each central zone type II hair cell, OCM emission intensity measurements were made from the optical section along the principal axis of the measured hair cell where the hair cell had the greatest area of OCM emission. A single mean OCM emission intensity among all the pixels within the defined circular area of each hair cell was subsequently extracted. Comparing the mean OCM emission intensities of the central zone hair cells to the threshold determined by the planar region hair cells enabled us to assign each measured central zone hair cell one of six different hair cell phenotypes: type Ic OCM+, type Id OCM+, type II OCM+, type Ic OCM-, type Id OCM-, and type II OCM-.

KCNQ4 expression analysis

KCNQ4 expression among central zone calyces was evaluated using the image processing program *FIJI*. High power 8-bit confocal image stacks of the central zone immunolabelled with CALB2, TUBB3, and KCNQ4 were imported into *FIJI*. The central zone within each confocal stack was delineated by identifying the region encompassing CALB2

immunolabelled calyces. KCNQ4 emission intensities of all central zone calyces of *Mus cristae* were measured. Since *Rousettus* has a greater number of central zone calyces compared to *Mus*, we collected emission intensity measurements from a sample of calyces for each *Rousettus* specimen. To determine which calyces to collect KCNQ4 emission intensity measurements from in *Rousettus*, all central zone calyces within confocal stacks were counted and assigned a number. After counting all central zone calyces within a confocal stack, calyces to collect measurements from were then randomly selected using a random number generator.

After the calyces from which to extract intensity measurements were randomly selected for in *Rousettus*, and all the central zone calyces identified in *Mus*, KCNQ4 emission intensities were then obtained. Using the single channel representative of KCNQ4 labelling, KCNQ4 emission intensities were obtained from a carefully chosen optical section of the confocal stacks where the KCNQ4 emission first creates a complete contour around each calyx, starting from the most apical section and navigating basally. Once the optical section was identified, KCNQ4 emission intensities were extracted by tracing a segmented contour 10 pixels in width around the inner face of each selected calyx where KCNQ4 expression was expected. Each traced contour was then converted into a straightened image that defines the area of the calyx from which KCNQ4 emission intensities per pixel will be extracted. From each straightened contour, a new 10-by-x (where x = contour perimeter in pixels) data array representing KCNQ4 emission intensities of 5 pixels on both sides of the traced contour was extracted for each calyx. After obtaining data arrays from each selected calyx, emission intensities were then parsed into 10-by-1 arrays for each pixel along the perimeter of the straightened contour, and the top 3 emission intensity values selected. Among the top KCNQ4 emission intensity values collected for each selected calyx, an aggregate median value was determined which would represent the KCNQ4

emission intensity level for that measured calyx. Using the channels representative of CALB2 and TUBB3 labelling, those representative median emission intensity values associated with CALB2-positive and CALB2-negative calyces were also recorded. Effectively, a dataset of representative median emission intensity values of both CALB2 expressing and non-expressing calyces were collected for each specimen.

Before pooling the *Rousettus* and *Mus* data, we normalized the representative median emission intensity values collected for each specimen in order to accommodate any variation in fixation, immunohistochemical processing, and imaging parameters between specimens. To normalize these values, first the median value of the native distribution of representative median emission intensity values was determined for each specimen. The native distribution of representative median emission intensity values was then divided by this single median value to create a normalized distribution of emission intensity values, where each of these new normalized values will be referred to from here on as the KCNQ4 intensity index (K.I.I.). This normalization was performed separately for each specimen, and the distribution of K.I.I.s were subsequently pooled.

To verify that KCNQ4 emission intensities measured from the sampled calyces were not subject to bleed-through caused by CALB2 emission, K.I.I.s were collected from randomly selected CALB2-positive and CALB2-negative central zone calyces in no primary control *Rousettus* and *Mus* specimens in which the KCNQ4 primary antibody was withheld. If CALB2 emission were detected in the channel representing KCNQ4 labelling in the confocal stacks, greater K.I.I.s associated with CALB2-positive calyces compared to CALB2-negative calyces would be observed. The K.I.I.s of CALB2-positive and CALB2-negative calyces are shown in Supplemental Fig. 2. A Kolmogorov-Smirnov test comparing these two populations of central

zone calyces was performed and revealed that the K.I.I.s of the CALB2-positive calyces were not significantly different than the CALB2-negative calyces ($P = 0.86$), verifying that CALB2 immunolabelling has no effect on the K.I.I.s obtained from central zone calyces.

Statistical Analysis

A bootstrap resampling strategy was implemented in the *R Studio statistical computing environment* to test hypotheses that empirical distributions of any tested characteristic from *Rousettus* could have resulted from random sampling of the underlying distribution as represented by *Mus*. This enabled generation of central zone hair cell and afferent phenotype distributions that were based on random resampling of the data collected from *Mus* and computation of explicit probabilities that the empirical *Rousettus* distributions could have resulted from random sampling from the *Mus* data. A random resampling of 1,000,000 trials were performed for each analysis in attempt to obtain explicit probabilities evaluating fractions of hair cell and afferent phenotypes. Significance was determined using an $\alpha = 0.05$. Analyses where native *Rousettus* distributions fell well outside of the resampled *Mus* distribution had probabilities expressed as an inequality (i.e. $P < 10^{-6}$). Rejection of these hypotheses ($P < 0.05$) would be indicative that the underlying factors driving the distributions of these hair cell and afferent phenotypes in each species are different.

Before testing hypotheses comparing distributions found in *Rousettus* and *Mus*, first we verified whether each experimental *Rousettus* specimen obtained for the study was representative of the underlying distributions of central zone hair cell or afferent phenotypes of the *Rousettus* species. A resampling strategy was performed to determine whether empirical distributions of any tested characteristic from any individual *Rousettus* specimen could have resulted from

random sampling of the pooled distribution collected from *Rousettus*. For all analyses, if each single experimental *Rousettus* specimen distribution fell within 95% of the two-tailed resampled distribution (e.g. $P > 0.05$), we would conclude that each individual *Rousettus* distribution was not significantly different from the pooled *Rousettus* distribution, and this would support pooling of the *Rousettus* data for the comparative analysis. The same strategy was repeated for *Mus* to validate the pooling of the *Mus* data. Examples of this verification strategy evaluating type I and type II hair cell fractions within the central zone of *Rousettus* and *Mus* horizontal cristae are shown in Supplementary Fig. 3.

For each analysis, we also determined whether any significant differences between the horizontal and superior cristae of each species existed. A resampling strategy was performed to determine whether empirical distributions of any tested characteristic from any individual superior crista specimen could have resulted from random sampling of the pooled distribution obtained from horizontal cristae. For all analyses, if each single experimental superior specimen distribution fell within 95% of the two-tailed resampled distribution (e.g. $P > 0.05$), we would conclude that each individual superior specimen distribution was not significantly different from the pooled horizontal cristae distribution, and this would support pooling of all *Rousettus* and all *Mus* data. If not, the data obtained from the horizontal and superior cristae would be analyzed separately. Any differences between the two crista types for either species were reported in the results.

For analysis of KCNQ4 expression among central zone calyces, we implemented a linear mixed-effects model in the *R statistical computing environment* to evaluate the fixed effects of species (i.e. *Rousettus* vs. *Mus*), CALB2 expression (i.e. expressing vs, non-expressing), and crista type (i.e. horizontal vs. superior) on K.I.I.s of central zone calyces, where *F* statistics were

determined for each fixed effect and their interactions. This mixed-effects model also included the random effect of animals (to account for non-independent measures obtained from different animals) on K.I.I.s. The native F statistics for each fixed effect and interaction were compared to a resampled distribution of F statistics obtained from random sampling of all K.I.I.s collected, allowing for computation of explicit probabilities that the native F statistics could have resulted from random sampling from the cumulative K.I.I. data. In the interest of limiting computation time, a total of 10,000 resampling trials were performed for this analysis and significance was determined using an $\alpha = 0.05$. If the native F statistic for any fixed effect fell within the lower 95% of the resampled distribution (i.e. $P > 0.05$), this would be indicative that the specified fixed effect does not influence K.I.I.s. Similarly, if the native F statistic of any interaction fell within the lower 95% of the resampled distribution (i.e. $P > 0.05$), this would be indicative that the fixed effects of that specified interaction are not inter-dependent on one another in their modulation of K.I.I.s.

RESULTS

***Rousettus* has a greater fraction of type I hair cells in the central zone than *Mus*.**

The data in Fig. 1 illustrate the distributions of type I and type II hair cells within the central zone of *Rousettus* and *Mus* cristae. Fig. 1A-D show low power sum slices projections of *Rousettus* and *Mus* horizontal and superior cristae with the central zone delineated by the presence of CALB2 immunolabelled calyces (green). Fig. 1E and 1F show high power sum slices projections illustrating type I and II hair cells present in *Rousettus* and *Mus*, respectively, where the type I hair cells are identified by the presence of a calyx (TUBB3, grayscale), while locations of type II hair cells are indicated by blue squares. Type I and type II hair cell counts and fractions are reported in Table 2. Since *Rousettus* has a greater number of hair cells than *Mus* (Table 2), fractions of type I and type II hair cells were compared.

Implementing the resampling strategy described in the methods section, we attempted to recreate the *Rousettus* distribution of central zone hair cells by sampling the *Mus* distribution to test the hypothesis that the fractions of type I and type II hair cells relative to all central zone hair cells in *Rousettus* and *Mus* are comparable. The resampled distributions of type I and type II hair cell fractions are illustrated by the boxplots in Fig. 1G, with the fractions of type I and type II hair cells obtained from individual *Rousettus* specimens identified by the open circles and open diamonds, respectively. From this resampling analysis, we were unable to derive the type I or type II hair cell fractions of *Rousettus* from the *Mus* distribution ($P < 10^{-6}$). Therefore, we reject the hypothesis that the fraction of type I and type II hair cells are comparable between *Rousettus* and *Mus*, with *Rousettus* having a greater fraction of type I hair cells and smaller fraction of type II hair cells. This finding suggests that the underlying factors driving the distributions of the type I and type II hair cells are different between *Rousettus* and *Mus*.

***Rousettus* and *Mus* have comparable fractions of type Ic and type Id hair cells, relative to all central zone type I hair cells.**

We compared the fractions of type Ic and type Id hair cells among total central zone type I hair cells in *Rousettus* and *Mus* to evaluate whether the increased fraction of type I hair cells in *Rousettus* was related to either of the type I hair cell subtypes. The data in Fig. 2 illustrate the distributions of type Ic and type Id hair cells in *Rousettus* and *Mus*. Fig. 2A and 2B show high power sum slices projections illustrating the subtypes of type I hair cells present in *Rousettus* and *Mus*, respectively, where type Ic hair cells can be identified by the presence of a calyx co-labelled for CALB2 (green) and TUBB3 (grayscale), and type Id hair cells can be identified by their association with a calyx labelled for only TUBB3 and are indicated by purple squares. Type Ic and type Id hair cell counts and fractions are reported in Table 2.

We attempted to recreate the *Rousettus* distribution of central zone type I hair cells by sampling the *Mus* distribution to test the hypothesis that the fractions of type Ic and type Id hair cells relative to all type I hair cells in *Rousettus* and *Mus* are comparable. However, in *Rousettus*, we found that the horizontal crista has a greater fraction of type Ic hair cells than the superior crista ($P = 0.03$). Therefore, the horizontal and superior data were analyzed separately when comparing type I hair cell subtypes. The resampled distributions of type Ic and type Id hair cell fractions of the horizontal and superior cristae are illustrated by the boxplots in Fig. 2D, with the fractions of type Ic (green) and type Id (red) hair cells obtained from individual *Rousettus* specimens identified by the open circles (horizontal crista) and open diamonds (superior crista). From this resampling analysis, we found that the probability of deriving the type Ic and type Id hair cell fractions of *Rousettus* from the *Mus* distribution is high for both

crista types (horizontal, $P = 0.53$; superior, $P = 0.44$). Therefore, we accept the hypothesis that the fractions of type Ic and type Id hair cells are comparable between *Rousettus* and *Mus*. This finding suggests that the underlying factors responsible for the distributions of the type I hair cell subtypes are similar in *Rousettus* and *Mus*.

OCM expression is strongly associated with type I hair cells in the central zone of both *Rousettus* and *Mus*. However OCM expression is exclusive to type I hair cells in *Rousettus*.

The data in Fig. 3 illustrate the distributions of OCM+ hair cells within the central zone of *Rousettus* and *Mus* cristae. Fig. 3A-D show low power sum slices projections of horizontal and superior cristae of *Rousettus* and *Mus* with visualization of OCM immunolabelled hair cells (red) distributed throughout the epithelia and the central zone delineated by the presence of CALB2 immunolabelled calyces (green). Counts and fractions of OCM+ hair cells in *Rousettus* and *Mus* are reported in Table 3.

First, we examined OCM expression among all central zone hair cells. We attempted to recreate the *Rousettus* distribution of OCM+ hair cells by sampling the *Mus* distribution to test the hypothesis that the fraction of OCM+ hair cells in *Rousettus* and *Mus* is comparable. However, in both species, we found a difference in OCM expression between the two crista types, with the horizontal crista having a greater fraction of hair cells that were OCM+ compared to the superior crista (*Rousettus*, $P = 0.0005$; *Mus*, $P = 0.05$). Due to this finding, the horizontal and superior data were analyzed separately. The resampled distributions of OCM+ hair cell fractions of the horizontal and superior cristae are illustrated by the boxplots in Fig. 3E, with the fractions of OCM+ hair cells obtained from individual *Rousettus* specimens identified by the open circles (horizontal crista) and open diamonds (superior crista). From this resampling

analysis, we found that the probability of deriving the OCM+ hair cell fraction of *Rousettus* from the *Mus* distribution is high for both crista types (horizontal, $P = 0.66$; superior, $P = 0.86$).

Therefore, we accept the hypothesis that the fraction of OCM+ hair cells in the central zone is comparable between *Rousettus* and *Mus*.

Since OCM expression is comparable between *Rousettus* and *Mus*, we examined whether OCM expression is random among hair cell types for each species. Fig. 4A-B show high power sum slices projections of *Rousettus* and *Mus*, respectively, where examples of different of OCM+ hair cell phenotypes are identified with colored arrows. First, we compared OCM expression in type I and type II hair cells in each species separately. Counts and fractions of OCM+ type I and II hair cells in *Rousettus* and *Mus* are reported in Table 3. We attempted to recreate the *Rousettus* distribution of OCM+ type I hair cells by sampling the *Rousettus* distribution of central zone hair cells to test the hypothesis that OCM expression among type I hair cells in *Rousettus* is random. We repeated this for *Mus* by attempting to recreate the *Mus* distribution of OCM+ type I hair cells by sampling the *Mus* distribution of central zone hair cells to test the hypothesis that OCM expression among type I hair cells in *Mus* is random. If the fraction of OCM+ type I hair cells was the result of random OCM expression among all central zone hair cells, we would expect the fraction of OCM+ type I hair cells relative to all OCM+ hair cells to be similar to the fraction of type I hair cells relative to all hair cells. The resampled distributions of OCM+ type I hair cell fractions of *Rousettus* and *Mus* are illustrated by the boxplots in Fig. 4C, with the fractions of OCM+ type I hair cells (relative to all OCM+ hair cells) obtained from individual specimens identified by the open circles (*Rousettus*) and open diamonds (*Mus*), respectively. From this resampling analysis, we were unable to derive the OCM+ type I hair cell fraction from total central zone hair cell distribution for either species (*Rousettus*, $P < 10^{-6}$; *Mus*,

$P = 0.0009$). Therefore, we reject the hypothesis that OCM expression among central zone hair cells is random in both *Rousettus* and *Mus*, and found that OCM expression is more closely associated with type I hair cells in both species.

Strikingly, we found that OCM expression in the central zone is virtually restricted to type I hair cells in *Rousettus*, with only 1 OCM+ type II hair cell encountered among three horizontal cristae, and 1 OCM+ type II hair cell encountered among three superior cristae. This is different from what we found in *Mus*, where a considerable fraction of OCM+ hair cells were type II hair cells (Table 3). It is evident that the underlying factors driving OCM expression towards type I hair cells in the central zone of *Rousettus* are not found in *Mus*.

OCM expression among central zone type I hair cell subtypes is comparable in *Rousettus* and *Mus*.

We evaluated whether OCM expression in central zone type I hair cells was related to either of the type I hair cell subtypes. Fig. 4A and 4B illustrate OCM expression (red) associated with the type I hair cell subtypes present in *Rousettus* and *Mus*, respectively. Counts and fractions of OCM+ type Ic and Id hair cells in *Rousettus* and *Mus* are reported in Table 3. We attempted to recreate the *Rousettus* distribution of OCM+ type Ic hair cells by sampling the *Rousettus* distribution of type I hair cells to test the hypothesis that OCM expression among type I hair cells in *Rousettus* is random. We repeated this separately for *Mus* by attempting to recreate the *Mus* distribution of OCM+ type Ic hair cells by sampling the *Mus* distribution of type I hair cells to test the hypothesis that OCM expression among type I hair cells in *Mus* is random. If the fraction of OCM+ type Ic hair cells were the result of random OCM expression among all type I hair cells, we would expect that the fraction of OCM+ type Ic hair cells relative to all OCM+

type I hair cells would be similar to the fraction of type Ic hair cells relative to all type I hair cells. The resampled distributions of OCM+ type Ic hair cell fractions of *Rousettus* and *Mus* are illustrated by the boxplots in Fig. 4D, with the fractions of OCM+ type Ic hair cells obtained from individual *Rousettus* and *Mus* specimens identified by the open circles and open diamonds, respectively. From this resampling analysis, we found that the probability of deriving the OCM+ type Ic hair cell fraction from total type I hair cell distribution was high for both species (*Rousettus*, $P = 0.92$; *Mus*, $P = 0.72$). Therefore, we accept the hypothesis that OCM expression among type I hair cell is random in both *Rousettus* and *Mus*. This finding suggests that the underlying factors responsible for OCM expression among central zone type I hair cell subtypes are similar in *Rousettus* and *Mus*.

***Rousettus* has a greater fraction of higher order complex calyces projecting to the central zone than *Mus*.**

Afferents associated with calyces (i.e. calyx-only and dimorphic afferents) can be further categorized based on the number of calyces associated with them. Those afferents with one calyx ending that receives input from a single type I hair cell are considered simple calyces or singlets. Those afferents with two or more calyces that receive input from two or more type I hair cells are considered complex calyces and are primarily found in the central zone (Fernández et al. 1988). Complex calyces can further be divided into doublets, triplets, quadruplets, and quintuplets, if associated with two, three, four, or five calyces, respectively. For this comparison, examination of differences was restricted to singlets, doublets, and triplets, since quadruplets and quintuplets were not found in *Mus*. Counts and fractions of simple and complex calyces of *Rousettus* and *Mus* are reported in Table 4.

We attempted to recreate the *Rousettus* distribution of calyces associated with singlets, doublets, and triplets relative to total central zone calyces by sampling the *Mus* distribution to test the hypothesis that the fractions of calyces associated with singlets, doublets, and triplets are comparable in *Rousettus* and *Mus*. From this resampling analysis, we were unable to derive the fraction of calyces associated with singlets in *Rousettus* from the *Mus* distribution ($P = 0.01$). Therefore, we reject the hypothesis that the fraction of calyces associated with singlets is comparable between *Rousettus* and *Mus*, and found that *Rousettus* has a smaller fraction of singlets. However, we found that the probability of deriving the fraction of calyces associated with doublets in *Rousettus* from the *Mus* distribution to be high ($P = 0.92$). Therefore, we accept the hypothesis that the fraction of calyces associated with doublets is comparable between *Rousettus* and *Mus*. When evaluating triplets, we found that the fraction of calyces associated with triplets was different in the two crista types of *Rousettus*, with the superior crista having a greater fraction than the horizontal ($P = 0.004$). Therefore, the horizontal and superior data were analyzed separately when comparing triplets. We were unable to derive the fraction of calyces associated with triplets in *Rousettus* from the *Mus* distribution for both crista types (horizontal, $P = 2.6e^{-05}$; superior, $P < 10^{-6}$). Therefore, we reject the hypothesis that the fraction of calyces associated with triplets is comparable between *Rousettus* and *Mus*, and found that *Rousettus* has a greater fraction of triplets. Higher order complex calyces such as quadruplets and quintuplets were found in *Rousettus* (188 total calyces associated with quadruplets from six *Rousettus* specimens, 10 total calyces associated with quintuplets found in a single *Rousettus* superior crista), but not in *Mus*. Overall, these findings suggest that the underlying factors responsible for the distribution of the simple and complex calyces are different in *Rousettus* and *Mus*. However, among complex calyces, it is evident that there are underlying factors polarizing the calyx-only

and dimorphic afferents towards triplets and higher complex calyces in *Rousettus* that are not present in *Mus*.

KCNQ4 emission among central zone calyces is comparable in *Rousettus* and *Mus*, but is associated with CALB2 expression in both species.

To evaluate any considerable differences in KCNQ4 expression of both species, crista types, and CALB2 phenotypes, a linear mixed-effects analytical model was implemented to test the hypothesis that K.I.I.s (a proxy measure for KCNQ4 expression) were similar in measures obtained from central zone calyces of *Rousettus* and *Mus*. The fixed effects under evaluation were defined as species (2 levels, *Rousettus* and *Mus*), crista type (2 levels, horizontal and superior), and CALB2 phenotype (2 levels, CALB2-positive and CALB2-negative). The additional random effect of animal (i.e. specimens) was defined to account for measurement non-independence between specimens. The distributions of K.I.I.s for all groups categorized by species, crista type, and CALB2 phenotype, are illustrated by the boxplots in Fig. 5C. The native F statistics for each fixed effect and their interactions was determined by performing ANOVAs on the linear mixed effect model. These native F statistics were compared to a resampled distribution of F statistics generated by random sampling of the pooled distribution of K.I.I.s to test the hypothesis that any specified fixed effect or interaction does not influence the distribution of K.I.I.s. From this analysis, we were unable to derive the native F statistic for the fixed effect of CALB2 phenotype from the resampled distribution of F statistics ($F = 220.26$; $P < 10^{-4}$). Thus we reject the hypothesis that the fixed effect of CALB2 phenotype does not influence the distribution of K.I.I.s, and found that CALB2-positive calyces having greater K.I.I.s than those CALB2-negative calyces. However, we found that the probabilities of deriving

the native F statistics for the fixed effect of species ($F = 0.78$; $P = 0.36$) and crista type ($F = 1.16$; $P = 0.27$) from the resampled distribution of F statistics are high. Thus we accept the hypotheses that the fixed effects of species and crista type do not influence the distribution of K.I.I.s.

This linear mixed effects model also enables us to evaluate any interaction between any of the fixed effects (i.e. whether the specified fixed effects are inter-dependent on one another) that may modulate K.I.I.s. From this analysis, we were unable to derive the native F statistic for the two-way interaction between the fixed effects of species and CALB2 phenotype ($F = 8.79$; $P = 0.005$) or the three-way interaction between the fixed effects of species, crista type, and CALB2 phenotype ($F = 13.39$, $P = 2e^{-04}$) from the resampled distribution of F statistics. Thus we reject the hypotheses that these interactions do not influence the distribution of K.I.I.s, and conclude that these interactions are inter-dependent on each other in their modulation of K.I.I.s. Evaluating the other possible interactions, we found that the probabilities of deriving the native F statistic for the two-way interaction between species and crista type ($F = 2.65$, $P = 0.10$) and for the two-way interaction between crista type and CALB2 phenotype ($F = 0.94$, $P = 0.33$) from the resampled distribution of F statistics are high. Thus we accept the hypotheses that these interactions do not influence the distribution of K.I.I.s, and conclude that these paired fixed effects are not inter-dependent on each other in their modulation of K.I.I.s.

DISCUSSION

The greater fraction of central zone type I hair cells reflects an adaptation in *Rousettus* that may be in response to increased agility.

The fraction of type I hair cells relative to all central zone hair cells of *Mus* found in the present study aligns with the findings of Desai et al. (2005). Therefore, our finding of a greater fraction of type I hair cells in the central zone of *Rousettus* compared to *Mus* is remarkable, and suggests that the factors driving the distribution of type I and type II hair cells in *Rousettus* and *Mus* are different. However, despite the greater fraction of type I hair cells in *Rousettus*, the distributions of type I hair cell subtypes (i.e. type Ic and Id) are comparable between *Rousettus* and *Mus*, suggesting that the underlying factors driving the expression of type I hair cell subtypes within the central zone are similar in both species and are not influenced by the unique behaviors of *Rousettus*.

The greater fraction of type I hair cells in the *Rousettus* central zone, directly translates to a greater presence of calyces associated with calyx-only and dimorphic afferents. Since the calyx-only and dimorphic afferents found to project to the central zone have irregular and phasic response characteristics (Baird et al. 1988), a greater presence of these afferents would enhance head movement coding by *Rousettus*. If the wing beat frequency of *Rousettus* (Riskin et al. 2010) is indicative of increased agile behavior and higher frequency head movement, the greater innervation by calyx-only and dimorphic afferents in the *Rousettus* central zone would represent a cellular adaptation that may serve to be advantageous for their flight behaviors.

Preferential OCM expression to type I hair cells in the central zone of *Rousettus* and OCM's possible presynaptic role for stimulus coding.

OCM expression among central zone hair cells is strikingly different between *Rousettus* and *Mus*. Despite *Rousettus* and *Mus* having comparable fractions of hair cells that express OCM, OCM expression is virtually absent in type II hair cells of *Rousettus*, while OCM expression is common among type II hair cells of *Mus*. Since OCM expression is restricted to type I hair cells in the central zone of *Rousettus*, we evaluated whether OCM expression among type I hair cell subtypes was comparable in the two species. However, we found that there was no preferential expression to either type I hair cell subtypes in both *Rousettus* and *Mus*, suggesting that the factors responsible for driving OCM expression in type I hair cells are the same in both species, but different in type II central zone hair cells. This finding aligns with the previous finding of a greater fraction of type I hair cells in *Rousettus* compared to *Mus*, but no difference in the fraction of type I hair cell subtypes between *Rousettus* and *Mus*.

Although the role of OCM within the vestibular sensory epithelia is not well understood, evaluating the functional role of another isoform of parvalbumin, α -parvalbumin, may help elucidate OCM's role. Acting as a calcium buffer, α -parvalbumin helps regulate calcium concentration in presynaptic terminals (Eggermann and Jonas 2011), which may help reduce the frequency of neurotransmitter release from these terminals, and thus temporally shorten the EPSPs of their associated postsynaptic terminals. Having shorter EPSPs enables the postsynaptic terminals to repolarize more quickly so that they are able to rapidly respond to the next presynaptic stimulus. OCM's role in cochlear outer hair cells has been studied and OCM has been shown to play an important role in auditory sensory transmission since OCM mutant mice demonstrate elevated ABR thresholds compared to wildtype mice (Tong et al. 2016). If

OCM plays a similar functional role within vestibular hair cells as in cochlear outer hair cells and as α -parvalbumin in other sensory systems, then OCM's enhanced expression among the greater fraction of type I hair cells found in the *Rousettus* central zone would be evidence of another cellular adaptation that may contribute to higher fidelity head movement coding in *Rousettus*.

The greater fraction of complex calyces, particularly those that are higher order, in *Rousettus* may be induced by their flight behaviors.

Desai et al. (2005) found that the distribution of simple calyces within the central zone was similar among terrestrial rodents, including *Mus*. However, we did not find this to be true in our comparison of simple calyces between *Rousettus* and *Mus*. In *Rousettus*, we found there to be a smaller fraction of central zone calyces that terminate as simple calyces compared to *Mus* (Table 4). When comparing the distributions of the subtypes of complex calyces, we found that the fraction of central zone calyces that terminate as doublets is comparable in *Rousettus* and *Mus*. However, differences emerge when evaluating higher order complex calyces. Not only did *Rousettus* have a greater fraction of central zone calyces that terminate in triplets compared to *Mus*, but quadruplets and quintuplets were only found in *Rousettus* and not in *Mus*. This finding shows that the greater fraction of type I hair cells found in the central zone of *Rousettus* is presented alongside the greater complexity of calyces that project to these type I hair cells.

The greater fraction of complex calyces in combination with the greater presence of higher order complex calyces that project to the central zone of *Rousettus* may contribute to the response dynamics of the central zone afferents necessary to accommodate the flight behaviors of *Rousettus*. Baird et al. (1988) estimates that each calyx terminal encompassing a type I hair

cell has three times the synaptic input of a bouton ending, suggesting that type I hair cells encompassed by complex calyces have a greater contribution to the discharge of calyx-only and dimorphic afferents than those type I hair cells encompassed by simple calyces. Studies evaluating the distribution of simple and complex calyces in other animals provide evidence that increased agility, particularly with flight behaviors, is correlated to greater complexity of calyces present in the crista epithelia. Birds are unique in having extremely large calyx terminals containing more type I hair cells on average (Haque, Huss and Dickman 2006) compared to those of mammals (Fernández et al. 1988; Fernández et al. 1995; Desai et al. 2005; Lysakowski and Goldberg 2008). Therefore, the greater presence of calyx-only and dimorphic afferents that terminate as complex calyces in central zone of *Rousettus* would result in alterations in head movement coding that could serve to accommodate the flight behaviors of *Rousettus*.

KCNQ4 expression is associated with CALB2 expression in central zone calyces of *Rousettus* and *Mus*.

The function of KCNQ4 as a postsynaptic modulator in the vestibular sensory epithelia has been well studied. Found in the inner face of calyces (Lysakowski et al. 2011; Spitzmaul et al. 2013), the low-voltage activated KCNQ4 channel serves to modulate the outward K⁺ current of the postsynaptic terminals of vestibular afferents. Therefore, these channels are critical for quick repolarization of the postsynaptic terminal directly after neurotransmitter release (Meredith and Rennie 2015), thus effectively shortening postsynaptic EPSPs and quickly preparing the postsynaptic membrane of afferents to respond to the next neurotransmitter release by type I hair cells. KCNQ4 channel expression is enhanced among calyces found in the central zone of mice

(Spitzmaul et al. 2013) and gerbils (Meredith and Rennie 2015) compared to those found in the peripheral zone, suggesting that KCNQ4 has a greater contribution to outward K⁺ currents in the central zone compared to the peripheral zone of rodents. Thus, the temporal coding advantage provided by the enhanced presence of KCNQ4 in central zone calyces may contribute to the faster postspike recovery of excitability demonstrated by the calyx-only and dimorphic afferents that project to the central zone (Baird et al. 1988).

We did not find a difference in K.I.I.s among central zone calyces between *Rousettus* and *Mus*, which suggests that *Rousettus* does not rely on the presence of KCNQ4 as an adaptation for enhanced head movement coding. However, we did find K.I.I.s to be strongly associated with postsynaptic CALB2 expression in the central zone calyces of both species, with CALB2-positive calyces having greater K.I.I.s than those central zone calyces that do not express CALB2. This association between CALB2 and KCNQ4 suggests that these two cellular markers share similar molecular mechanisms that are responsible for their expression among central zone calyces in the crista epithelia. Therefore, it is possible that the greater presence of KCNQ4 in CALB2-positive calyces may contribute to the response dynamics of calyx-only afferents that differ to those of dimorphic afferents projecting to the central zone.

Differences between crista types in *Rousettus* and *Mus*.

In both *Rousettus* and *Mus*, there were instances in which the horizontal crista displayed distributions of central zone hair cell and afferent phenotypes that differed to those of the superior crista. We found that the distributions of type I, type II, and type I subtypes within the central zone of both the horizontal and superior cristae of *Mus* were the same, which supports the

findings of Desai et al. (2005) (Table 2). However, differences between the two crista types were apparent when evaluating total number of central zone hair cells (Table 2) in both *Rousettus* and *Mus*, OCM expression among central zone hair cells in both *Rousettus* and *Mus* (Fig. 3, Table 3), and the distribution of complex calyces in *Rousettus* (Table 4). In *Mus*, as shown in Fig. 1D, the superior crista has a special anatomical feature located at the midpoint called the eminentia cruciatum where there is an absence of hair cells and nerve fibers (Desai et al. 2005). However, neither the horizontal crista of *Mus* (Fig. 1B) or the horizontal and superior cristae of *Rousettus* (Fig. 1A, C) have an eminentia cruciatum. Since *Rousettus* displays more differences between the two crista types than *Mus*, the presence of an eminentia cruciatum is unlikely to be the sole driver of any differences that were found between the horizontal and superior cristae. It would be valuable to supplement the present study's findings with physiological and behavioral data (such as recordings from vestibular afferents in *Rousettus* and recordings of their natural head movements in flight) in order to provide insight into the functional role of these cellular adaptations in the different crista types of *Rousettus*.

FIGURES

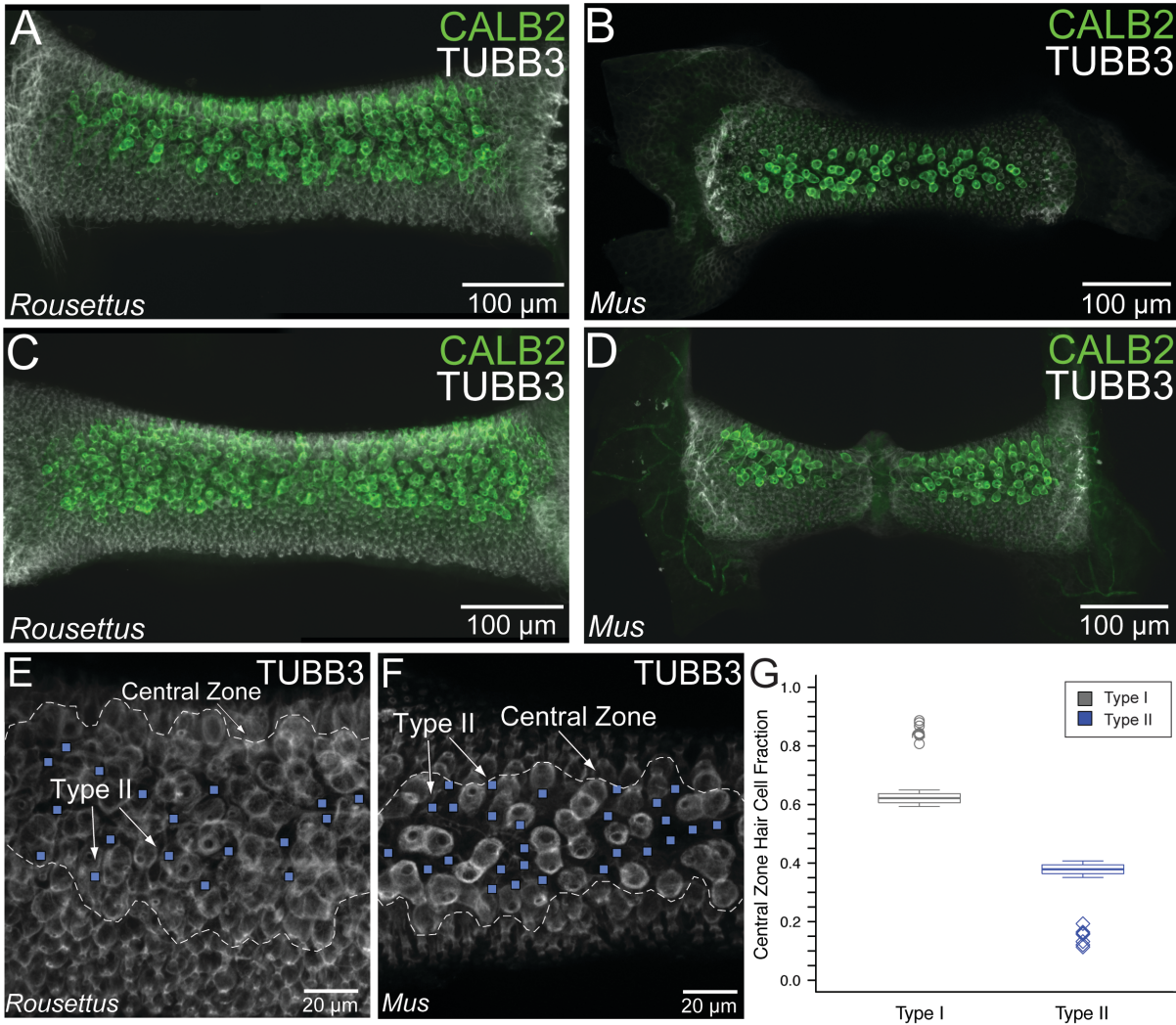


Figure 1. *Roussettus* has a greater fraction of type I hair cells in the central zone. *A-D*: Low power sum slices projections of horizontal and superior cristae from *Roussettus* taken at 1.4x zoom (*A, C*) and *Mus* taken at 1.5x zoom (*B, D*), respectively. Scale bars were placed on confocal images by calculating μm/pixel ratios. CALB2 expressing calyces (green) demarcate the central zone of the epithelia in both species. *E-F*: High power sum slices projections of the central zone (dashed line), in *Roussettus* (*E*) and *Mus* (*F*). Type I hair cells are associated with calyces labelled with TUBB3 (grayscale). Type II hair cells (blue squares) not associated with a calyx were identified by PHAL staining (not shown). *G*: Using resampling analysis, we tested the hypothesis that the fractions of type I and II hair cells (relative to all central zone hair cells) are similar in *Roussettus* and *Mus*. Boxplots represent the resampled distributions of type I (gray) and type II (blue) hair cell fractions (relative to all central zone hair cells) sampled from the native pooled *Mus* distribution of central zone hair cells. Open circles (gray) reflect type I and open diamonds (blue) reflect type II fractions obtained from individual *Roussettus* specimens. This analysis shows that the fraction of type I hair cells relative to total central zone hair cells is greater in *Roussettus*. Since the full complement of central zone hair cells is comprised of either type I or type II hair cells, we also conclude that the fraction of type II hair cells relative to total central zone hair cells is lower in *Roussettus* ($P < 10^{-6}$).

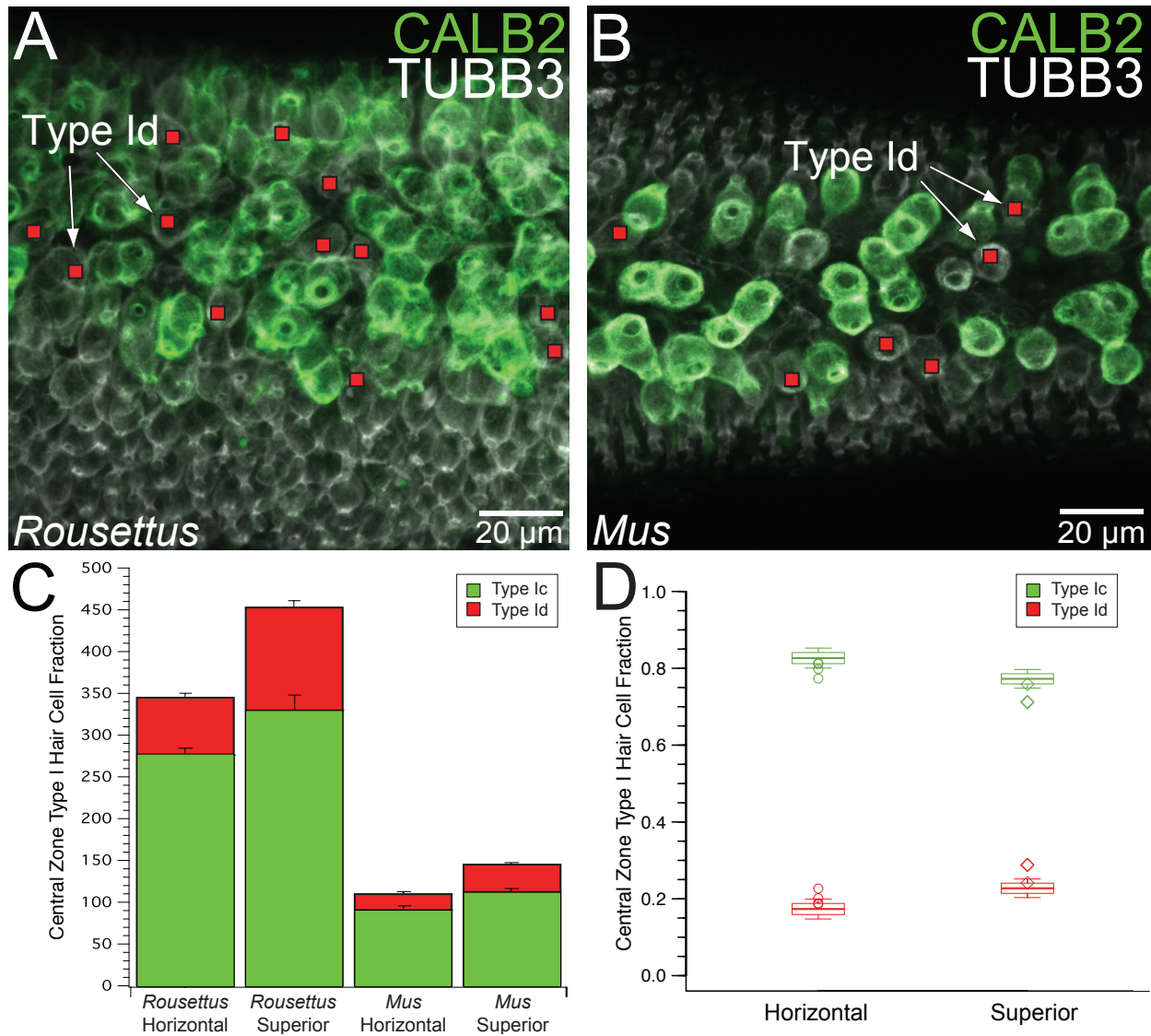


Figure 2. Distributions of type I hair cell subtypes in the central zone are comparable in *Roussettus* and *Mus*.

A-B: High power sum slices projections of the central zone in *Roussettus* (*A*) and *Mus* (*B*). Scale bars were placed on confocal images by calculating $\mu\text{m}/\text{pixel}$ ratios. CALB2 expressing calyces (green) demarcate the central zone. Type Ic hair cells are associated with calyces that are co-localized for TUBB3 (grayscale) and CALB2, while type Id hair cells (red squares) are associated with calyces that are labelled for TUBB3 only. *C*: There are more central zone type I hair cells in *Roussettus* than in *Mus*, but both *Roussettus* and *Mus* display a greater number of type Ic than type Id hair cells in the central zone. *D*: Using resampling analysis, we tested the hypothesis that the fractions of type Ic and Id hair cells (relative to all central zone type I hair cells) are similar in *Roussettus* and *Mus*. Since the horizontal and superior cristae of *Roussettus* had different fractions of type Ic hair cells (not shown, $P = 0.03$), the horizontal and superior data were analyzed separately when comparing type I hair cell subtypes between *Roussettus* and *Mus*. Boxplots represent the distributions of type Ic (green) and type Id (red) hair cell fractions sampled from the native distribution of the *Mus* central zone type I hair cells pooled from horizontal (left) and superior cristae (right). Open circles (horizontal) and open diamonds (superior) reflect type Ic (green) and type Id (red) fractions obtained from individual *Roussettus* specimens. This analysis shows that the fractions of type Ic and type Id hair cells in *Roussettus* and *Mus* are comparable in both crista types (horizontal, $P = 0.53$; superior, $P = 0.44$).

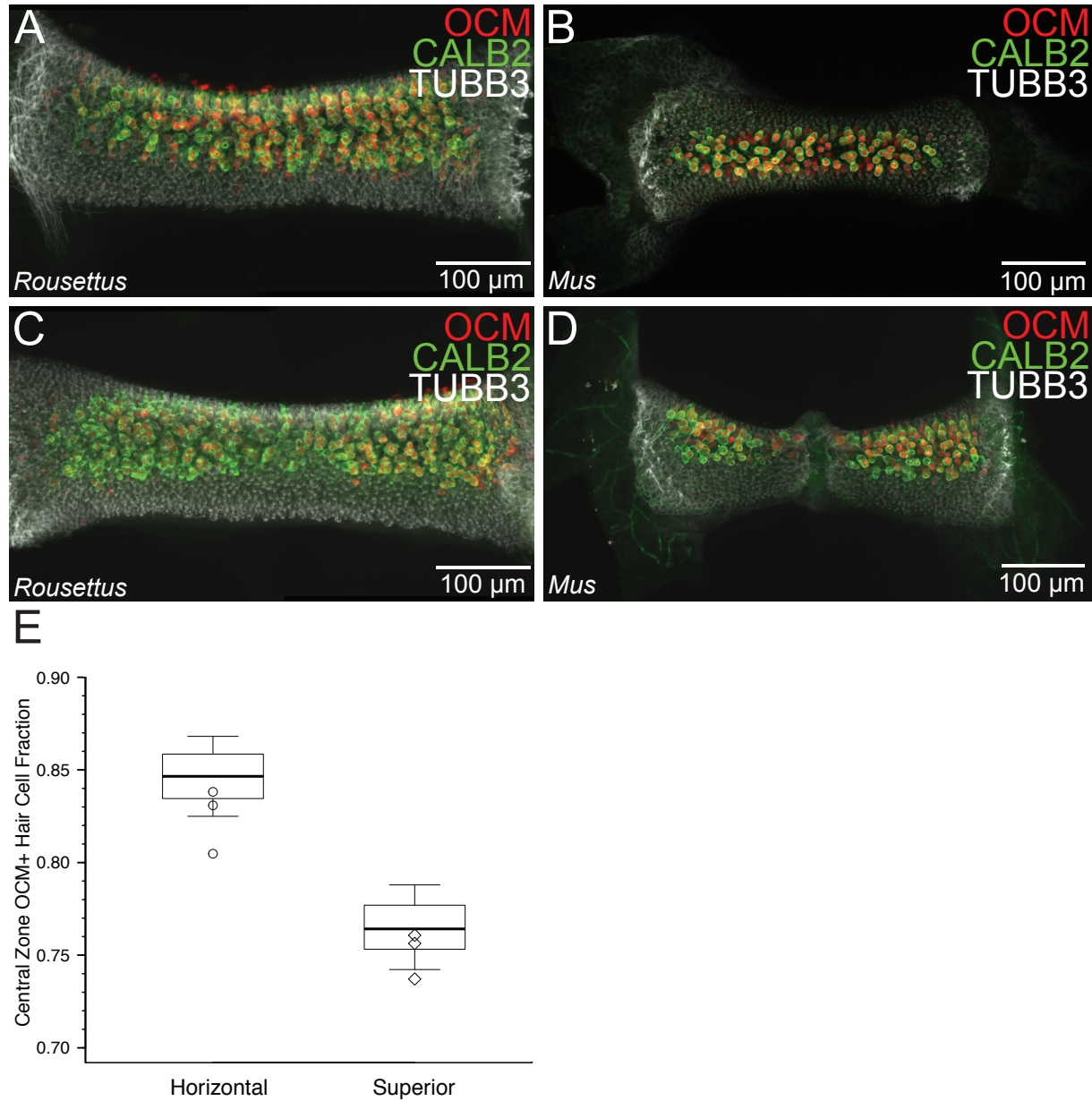


Figure 3. OCM expression among central zone hair cells is comparable in *Rousettus* and *Mus*. *A-D*: Low power sum slices projections of horizontal and superior cristae from *Rousettus* taken at 1.4x zoom (*A, C*) and *Mus* taken at 1.5x zoom (*B, D*), respectively. Scale bars were placed on confocal images by calculating $\mu\text{m}/\text{pixel}$ ratios. OCM expression (red) is localized to the central zone (green). *E*: Using resampling analysis, we tested the hypothesis that the fractions of OCM+ hair cells (relative to all central zone hair cells) are similar in *Rousettus* and *Mus*. Since the horizontal and superior cristae of both *Rousettus* and *Mus* had different fractions of OCM+ hair cells (not shown; *Rousettus*, $P < 10^{-3}$; *Mus*, $P = 0.05$), the horizontal and superior data were analyzed separately when comparing OCM+ hair cells between *Rousettus* and *Mus*. Boxplots represent the resampled distributions of OCM+ hair cell fractions sampled from the native distribution of *Mus* central zone hair cells pooled from horizontal (left) and superior (right) cristae. Open circles and open diamonds reflect OCM+ fractions obtained from individual *Rousettus* horizontal and superior cristae, respectively. This analysis shows that the fraction of OCM+ hair cells in *Rousettus* and *Mus* is comparable in both crista types (horizontal, $P = 0.66$; superior, $P = 0.86$).

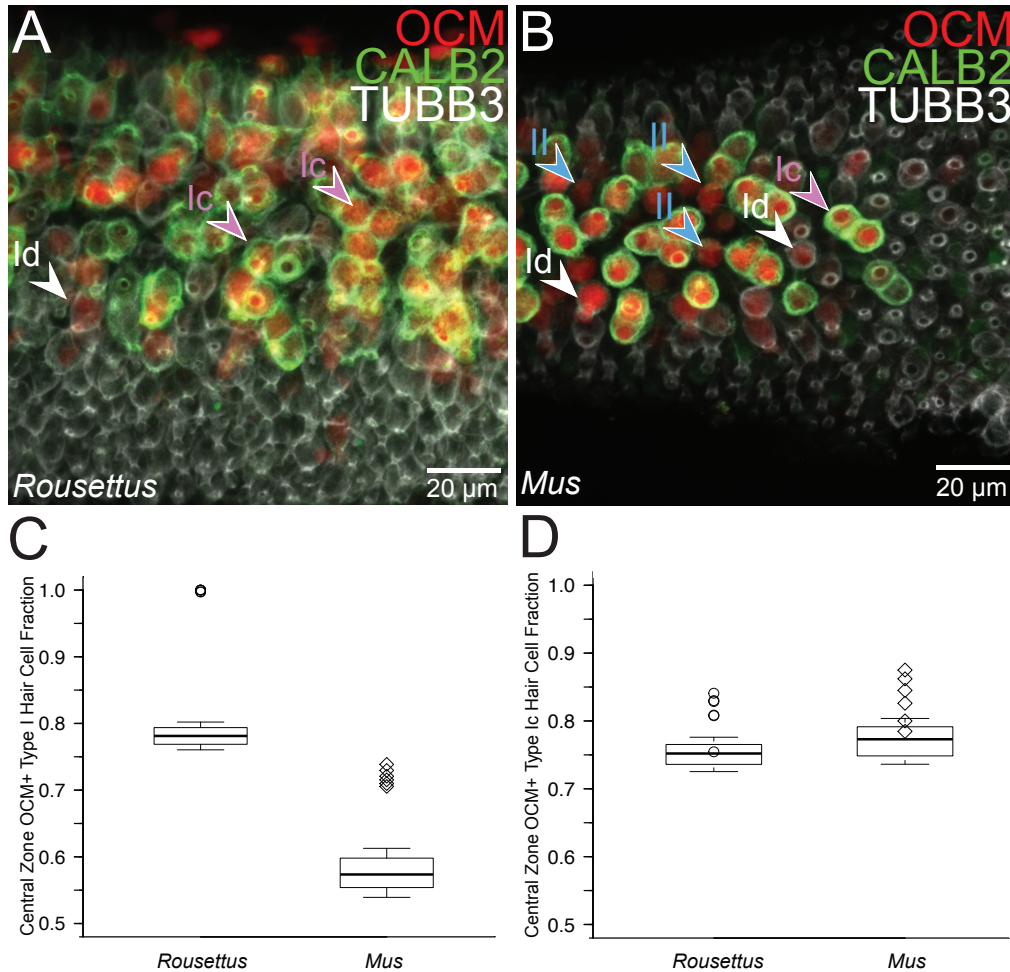


Figure 4. OCM expression among central zone type I hair cells is comparable in *Rousettus* and *Mus*. *A-B*: High power sum slices projections of the central zone of *Rousettus* (*A*) and *Mus* (*B*). Scale bars were placed on confocal images by calculating $\mu\text{m}/\text{pixel}$ ratios. Examples of various hair cell phenotypes are identified by arrows: purple arrows identify OCM+ type Ic hair cells which are associated with a calyx that is co-localized for CALB2 (green) and TUBB3 (grayscale); white arrows identify OCM+ type Id hair cells which are associated with a calyx that is labelled for only TUBB3; blue arrows identify OCM+ type II hair cells which can be identified by lack of a calyx. OCM+ type II hair cells are less common in *Rousettus* compared to *Mus*. *C*: We tested the hypothesis that OCM expression is random among central zone hair cells for each species. If OCM expression was random, the fraction of OCM+ type I hair cells (relative to all central zone OCM+ hair cells) would be comparable to the native fraction of type I hair cells (relative to all central zone hair cells). Boxplots represent the resampled distributions of OCM+ type I hair cell fractions sampled from the native pooled distribution of *Rousettus* (left) and *Mus* (right) central zone hair cells. Open circles and open diamonds reflect OCM+ type I fractions from individual *Rousettus* and *Mus* specimens, respectively. This analysis shows that OCM expression is more closely associated with type I hair cells in both *Rousettus* and *Mus* (*Rousettus*, $P < 10^{-6}$; *Mus*, $P = 0.0009$). *D*: We tested the hypothesis that OCM expression in the central zone is random among type I hair cells. If OCM expression was random, the fraction of OCM+ type Ic hair cells (relative to all central zone OCM+ type I hair cells) would be comparable to the native fraction of type Ic hair cells (relative to all central zone type I hair cells). Boxplots represent the resampled distributions of OCM+ type Ic hair cell fractions sampled from the native pooled distribution of *Rousettus* (left) and *Mus* (right) central zone type I hair cells. Open circles and open diamonds reflect OCM+ type Ic fractions from individual *Rousettus* and *Mus* cristae, respectively. This analysis shows that in both *Rousettus* and *Mus*, OCM expression among type I hair cells is random (*Rousettus*, $P = 0.92$; *Mus*, $P = 0.72$).

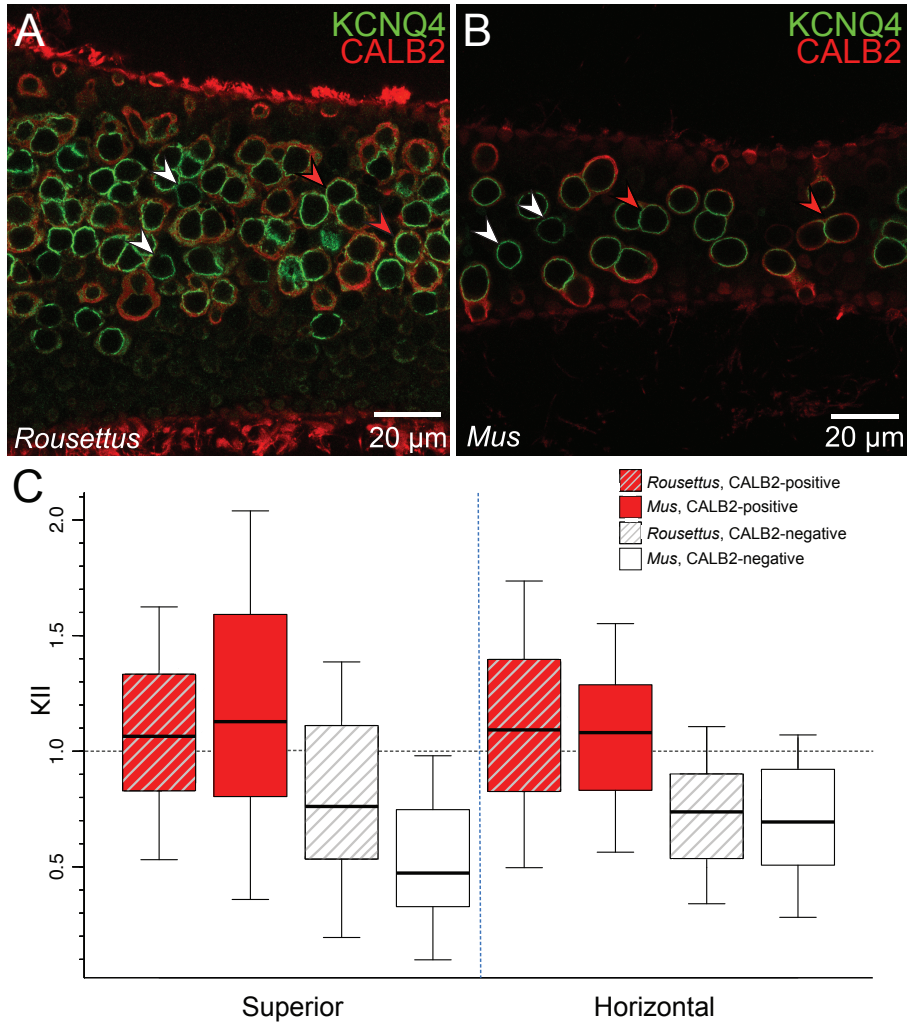


Figure 5. KCNQ4 emission is associated with CALB2 phenotype among central zone calyces of both *Roussettus* and *Mus*. *A-B*: High power optical sections of the central zone of *Roussettus* (*A*) and *Mus* (*B*). Scale bars were placed on confocal images by calculating $\mu\text{m}/\text{pixel}$ ratios. CALB2 expressing calyces are identified in red (with examples identified by red arrows), while any calyces immunolabelled with KCNQ4 (green), but not CALB2 are identified as CALB2-negative calyces (with examples identified by white arrows). *C*: We examined the fixed effect factors of species (i.e. *Roussettus* vs. *Mus*), crista type (i.e. horizontal vs. superior), and CALB2 phenotype (i.e. CALB2-positive, red; CALB2-negative, white) on K.I.I.s among central zone calyces. Boxplots show the distributions of K.I.I.s (a proxy measure for KCNQ4 expression) obtained from central zone calyces from groups categorized by species (*Roussettus*, patterned; *Mus*, non-patterned), crista type (superior, right; horizontal, left), and CALB2 phenotype (CALB2-positive, red; CALB2-negative, white). The native F statistics for each fixed effect was determined and compared to a resampled distribution of F statistics generated by random sampling of the pooled distribution of K.I.I.s to test the hypothesis that the native F statistic for any fixed effect or their interactions could have resulted from random sampling from the cumulative K.I.I. data. This resampling analysis showed that the fixed effect of CALB2 phenotype has a considerable impact on K.I.I.s measured from central zone calyces of both *Roussettus* and *Mus*, with CALB2 expressing calyces have greater K.I.I.s than those central zone calyces that do not express ($F = 220.26$; $P < 10^{-4}$). However, the fixed effects of species ($F = 0.78$; $P = 0.36$) and crista type ($F = 1.16$; $P = 0.36$) do not. When evaluating the possible interaction between the fixed effects of species, crista type, and CALB2 phenotype, we found that there was a significant 2-way interaction between species and CALB2 phenotype ($F = 8.79$, $P = 0.005$), and 3-way interaction between species, crista type, and CALB2 phenotype ($F = 13.39$, $P = 2e^{-04}$), but no significant 2-way interaction between species and crista type ($F = 2.65$, $P = 0.10$) or crista type and CALB2 phenotype ($F = 0.94$, $P = 0.33$).

TABLES

Table 1: Primary and Secondary Antibodies							
<i>Rousettus</i> and <i>Mus</i> Cristae with OCM							
1° Ab	Conc.	Manufacturer	Product #	2° Ab/Stains	Conc.	Manufacturer	Product #
Ms x CALB2	1:250	Millipore	MAB1568	Dk x Ms AF488	1:250	Life Technologies	A21202
Gt x OCM	1:250	Santa Cruz Biotech	SC-7446	Dk x Gt AF555	1:250	Life Technologies	A31573
Rb x TUBB3	1:250	Biologend	PRB-435P	Dk x Rb AF647	1:250	Life Technologies	A111056
				Phalloidin CF405	1:100	Biotium	00034
<i>Rousettus</i> and <i>Mus</i> Cristae with KCNQ4							
1° Ab	Conc.	Manufacturer	Product #	2° Ab/Stains	Conc.	Manufacturer	Product #
Ms x KCNQ4	1:100	Santa Cruz Biotech	SC-271320	Dk x Ms AF488	1:250	Life Technologies	A21202
Gt x CALB2	1:250	Millipore	AB11550	Dk x Gt AF555	1:250	Life Technologies	A31573
				Dk x Gt AF546	1:250	Life Technologies	A10040
Rb x TUBB3	1:250	Biologend	PRB-435P	Dk x Rb AF647	1:250	Life Technologies	A111056
				Phalloidin CF405	1:200	Biotium	00034

Table 2: Central Zone Hair Cells							
Number of Central Zone Hair Cells							
Species	n	Crista Type	Total	Type I	Type II	Type Ic	Type Id
<i>Rousettus</i>	4	Horizontal	398 ± 29	346 ± 23	53 ± 11	276 ± 17	70 ± 9
<i>Rousettus</i>	3	Superior	547 ± 29	453 ± 34	93 ± 5	330 ± 31	123 ± 13
<i>Mus</i>	5	Horizontal	178 ± 19	110 ± 13	68 ± 8	91 ± 10	19 ± 5
<i>Mus</i>	3	Superior	233 ± 12	146 ± 6	88 ± 6	113 ± 7	33 ± 3
Fraction of Central Zone Hair Cells							
Species	n	Crista Type	Type I/Total	Type II/Total	Type Ic/Total I	Type Id/Type I	
<i>Rousettus</i>	4	Horizontal	0.87 ± 0.02	0.13 ± 0.02	0.80 ± 0.02	0.20 ± 0.02	
<i>Rousettus</i>	3	Superior	0.83 ± 0.02	0.16 ± 0.02	0.73 ± 0.03	0.27 ± 0.03	
<i>Mus</i>	5	Horizontal	0.62 ± 0.02	0.38 ± 0.02	0.83 ± 0.03	0.17 ± 0.03	
<i>Mus</i>	3	Superior	0.62 ± 0.01	0.38 ± 0.01	0.77 ± 0.02	0.23 ± 0.02	
All values are means ± SD. n, number of cristae.							

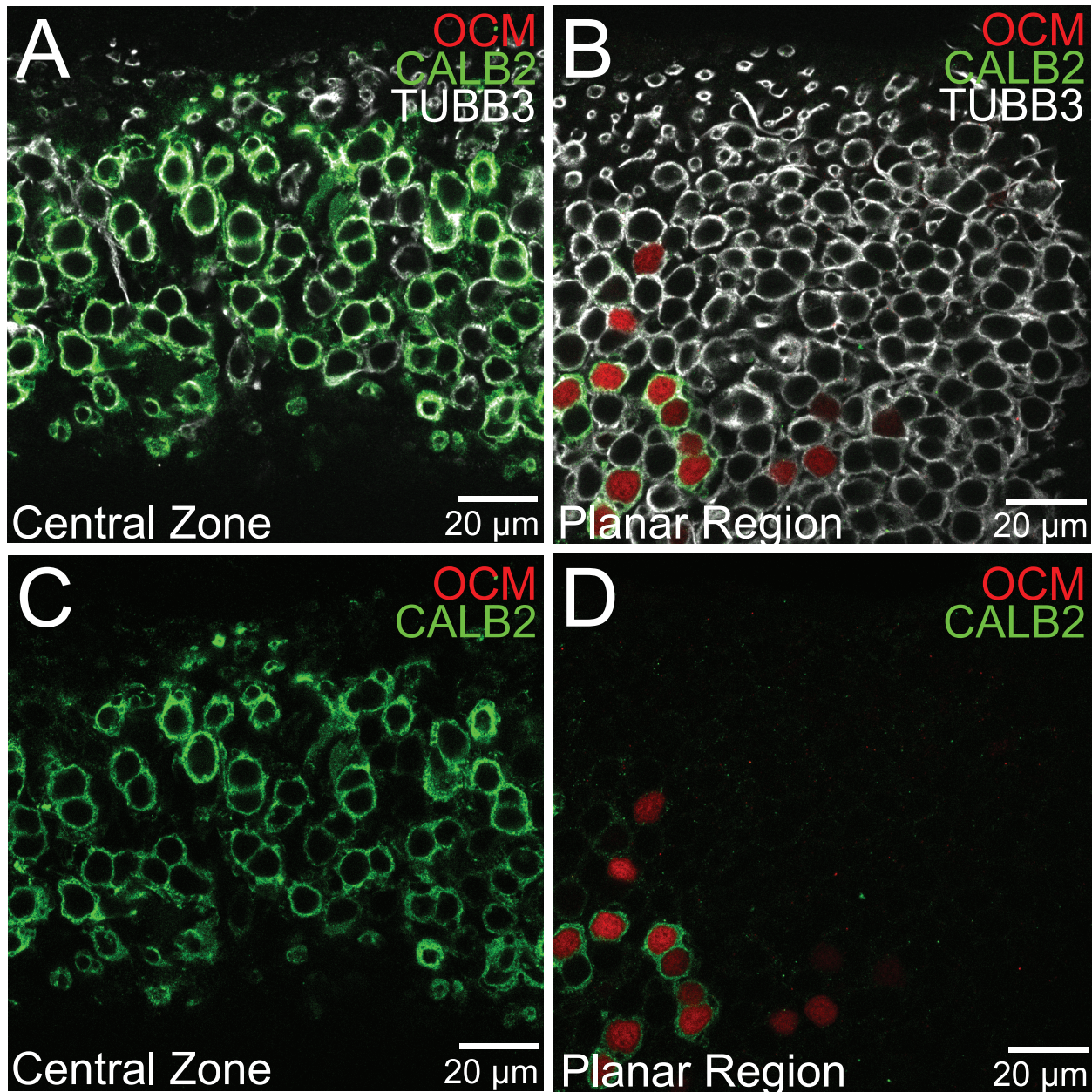
Table 3: OCM+ Central Zone Hair Cells								
Number of OCM+ Central Zone Hair Cells								
Species	<i>n</i>	Crista	Total	Total OCM+	Total OCM+ Type I	Total OCM+ Type Ic	Total OCM+ Type Id	Total OCM+ Type II
<i>Rousettus</i>	3	Horizontal	417 ± 9	343 ± 7	343 ± 7	281 ± 8	62 ± 6	0.3 ± 0.6
<i>Rousettus</i>	3	Superior	547 ± 29	411 ± 20	410 ± 20	327 ± 32	83 ± 11	0.3 ± 0.6
<i>Mus</i>	3	Horizontal	175 ± 25	148 ± 22	106 ± 16	91 ± 12	16 ± 5	42 ± 6
<i>Mus</i>	3	Superior	234 ± 12	179 ± 17	129 ± 13	105 ± 15	24 ± 3	50 ± 4
Fraction of OCM+ Central Zone Hair Cells								
Species	<i>n</i>	Crista	OCM+/ Total	OCM+ Type I/ Total OCM+	OCM+ Type II/ Total OCM+	OCM+ Type Ic/ OCM+ Type I	OCM+ Type Id/ OCM+ Type I	
<i>Rousettus</i>	3	Horizontal	0.83 ± 0.02	1.00 ± 0.00	0.00 ± 0.00	0.83 ± 0.02	0.17 ± 0.02	
<i>Rousettus</i>	3	Superior	0.75 ± 0.01	1.00 ± 0.00	0.00 ± 0.00	0.80 ± 0.04	0.20 ± 0.04	
<i>Mus</i>	3	Horizontal	0.84 ± 0.03	0.72 ± 0.01	0.28 ± 0.01	0.85 ± 0.03	0.15 ± 0.03	
<i>Mus</i>	3	Superior	0.76 ± 0.04	0.72 ± 0.02	0.28 ± 0.02	0.81 ± 0.03	0.19 ± 0.03	

All values are means ± SD. *n*, number of cristae.

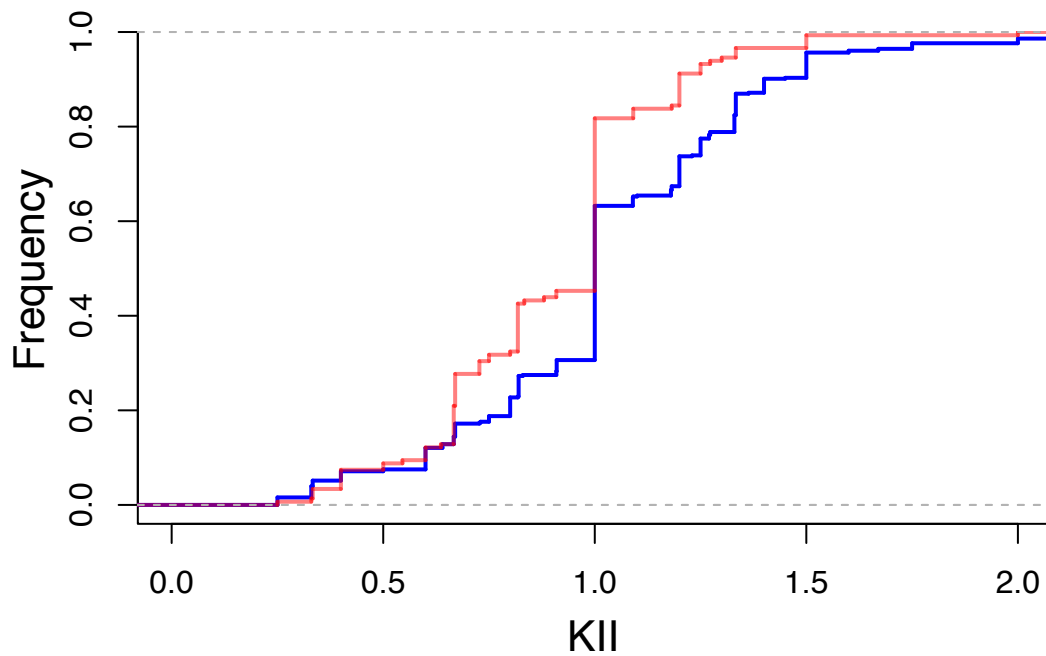
Table 4: Central Zone Simple and Complex Calyces							
Number of Central Zone Calyces							
Species	<i>n</i>	Crista	Total	Singlets	Doublets	Triplets	Quadruplets
<i>Rousettus</i>	3	Horizontal	358 ± 9	121 ± 9	150 ± 26	64 ± 20	21 ± 27
<i>Rousettus</i>	3	Superior	453 ± 34	141 ± 5	143 ± 23	124 ± 24	41 ± 32
<i>Mus</i>	5	Horizontal	110 ± 13	49 ± 8	56 ± 7	6 ± 6	0
<i>Mus</i>	3	Superior	146 ± 6	60 ± 5	71 ± 1	15 ± 5	0
Fraction of Central Zone Calyces							
Species	<i>n</i>	Crista	Singlets/ Total	Doublets/ Total	Triplets/ Total	Quadruplets/ Total	
<i>Rousettus</i>	3	Horizontal	0.34 ± 0.03	0.42 ± 0.08	0.18 ± 0.05	0.05 ± 0.07	
<i>Rousettus</i>	3	Superior	0.31 ± 0.03	0.32 ± 0.07	0.27 ± 0.03	0.08 ± 0.07	
<i>Mus</i>	5	Horizontal	0.43 ± 0.04	0.50 ± 0.02	0.06 ± 0.05	0	
<i>Mus</i>	3	Superior	0.41 ± 0.03	0.49 ± 0.02	0.02 ± 0.03	0	

All values are means ± SD. *n*, number of cristae.

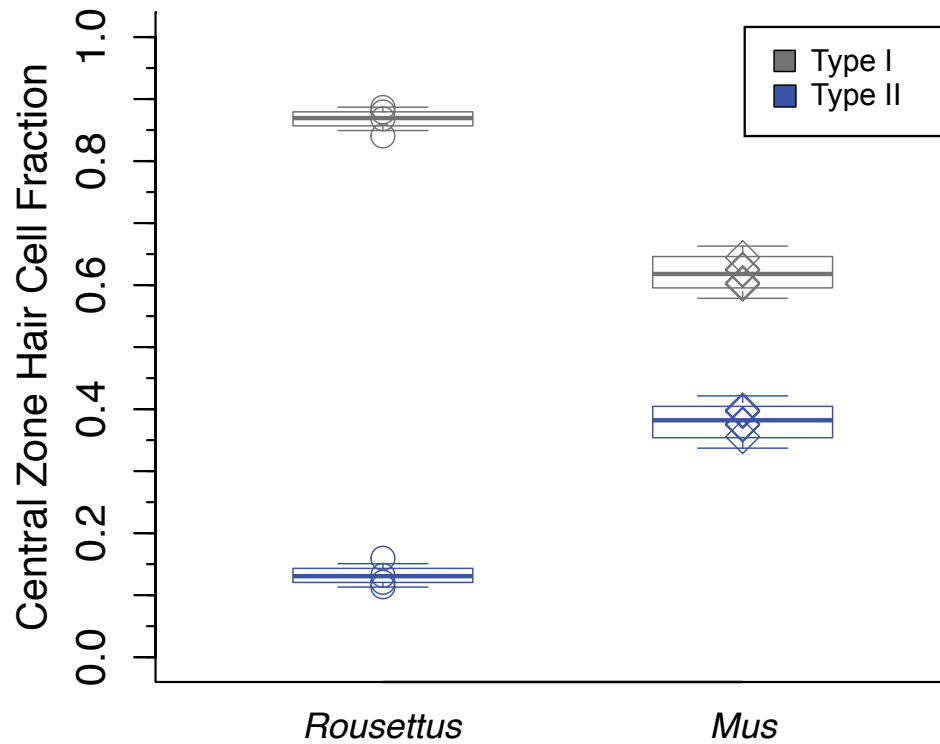
APPENDIX: SUPPLEMENTAL FIGURES



Supplemental Figure 1. Determining OCM emission threshold for positive expression. OCM emission intensities of hair cells in the planar region is greater than those hair cells in the central zone of no primary OCM control specimens. *A-D*: High power optical sections taken from the central zone (*A,C*) and planar region (*B, D*) of *Rousettus*. Scale bars were placed on confocal images by calculating $\mu\text{m}/\text{pixel}$ ratios. The no primary OCM control specimens in which the primary antibody against OCM was omitted from its immunoprocessing, is shown with TUBB3 (grayscale) overlaid (*A*) and without (*C*), and was imaged in the central zone, identified by the region encompassing CALB2 (green) expressing calyces, and where OCM (red) expression was expected. The specimen in which the primary antibody against OCM was included in its immunoprocessing, is shown with TUBB3 overlaid (*B*) and without (*D*), and was imaged in the planar region located just outside of the central zone, where OCM expression was not expected. The level of OCM emission intensity in hair cells found in the planar region of the OCM labeled specimen was higher compared to those found in the central zone of the no primary control specimen, justifying sampling from planar region hair cells of the OCM labeled specimens to establish the threshold of OCM+ positive expression.



Supplemental Figure 2. K.I.I.s of CALB2-positive and CALB2-negative calyces are comparable in no primary KCNQ4 control specimens. The normalized cumulative distribution of K.I.I.s of CALB2-positive (blue) and CALB2-negative (red) central zone calyces pooled from three *Rousettus* and three *Mus* no primary KCNQ4 control specimens. Implementation of a two-sample Kolmogorov-Smirnov test comparing these two populations of central zone calyces revealed that the distribution of K.I.I.s of the CALB2-positive calyces was not significantly greater than that of the CALB2-negative calyces ($P = 0.86$), verifying that CALB2 immunolabelling has no effect on the K.I.I.s obtained from CALB2-positive central zone calyces.



Supplemental Figure 3. Example verification of the pooling of *Roussettus* and *Mus* data evaluating type I and type II hair cell fractions within the central zone of horizontal crista. The boxplots represent 1,000,000 resampled distributions of type I (grey) and type II hair cells (blue) fractions relative to all central zone hair cells sampled from the native pooled distribution of *Roussettus* (left) and *Mus* (right) central zone hair cells from horizontal crista, where the lower and upper whiskers identify the 10th and 90th percentile, and the lower and upper hinges identify the 25th and 75th percentile of the distribution, respectively. Open circles identify the fractions of type I hair cells (gray) and type II hair cells (blue) relative to all central zone hair cells for each individual *Roussettus* crista analyzed, while open diamonds identify the fractions of type I hair cells (gray) and type II hair cells (blue) relative to all central zone hair cells for each individual *Mus* horizontal crista analyzed. Each individual specimen's distribution of type I and type II hair cells was not significantly different from the respective species pooled distribution ($P = 0.11$, $P = 0.98$, $P = 0.56$, $P = 0.30$ for *Roussettus* specimens 1-4, respectively; and $P = 0.65$, $P = 0.65$, $P = 0.87$, $P = 0.87$, $P = 0.53$ for *Mus* specimens 1-5, respectively).

REFERENCES.

- Baird, R. A., G. Desmadryl, C. Fernández & J. M. Goldberg (1988) The vestibular nerve of the chinchilla. II. Relation between afferent response properties and peripheral innervation patterns in the semicircular canals. *J Neurophysiol*, 60, 182-203.
- Davies, K. T., P. J. Bates, I. Maryanto, J. A. Cotton & S. J. Rossiter (2013) The evolution of bat vestibular systems in the face of potential antagonistic selection pressures for flight and echolocation. *PLoS One*, 8, e61998.
- Desai, S. S., H. Ali & A. Lysakowski (2005) Comparative morphology of rodent vestibular periphery. II. Cristae ampullares. *J Neurophysiol*, 93, 267-80.
- Desmadryl, G. & C. J. Dechesne (1992) Calretinin immunoreactivity in chinchilla and guinea pig vestibular end organs characterizes the calyx unit subpopulation. *Exp Brain Res*, 89, 105-8.
- Eggermann, E. & P. Jonas (2011) How the 'slow' Ca(2+) buffer parvalbumin affects transmitter release in nanodomain-coupling regimes. *Nat Neurosci*, 15, 20-2.
- Engstrom, H. (1961) The innervation of the vestibular sensory cells. *Acta Otolaryngol Suppl*, 163, 30-41.
- Fernández, C., R. A. Baird & J. M. Goldberg (1988) The vestibular nerve of the chinchilla. I. Peripheral innervation patterns in the horizontal and superior semicircular canals. *J Neurophysiol*, 60, 167-81.
- Fernández, C., A. Lysakowski & J. M. Goldberg (1995) Hair-cell counts and afferent innervation patterns in the cristae ampullares of the squirrel monkey with a comparison to the chinchilla. *J Neurophysiol*, 73, 1253-69.
- Goldberg, J. M., G. Desmadryl, R. A. Baird & C. Fernández (1990) The vestibular nerve of the chinchilla. V. Relation between afferent discharge properties and peripheral innervation patterns in the utricular macula. *J Neurophysiol*, 63, 791-804.
- Hadziselimovic, H. & L. J. Savkovic (1964) Appearance of semicircular canals in birds in relation to mode of life. *Acta Anat (Basel)*, 57, 306-15.
- Haque, A., D. Huss & J. D. Dickman (2006) Afferent innervation patterns of the pigeon horizontal crista ampullaris. *J Neurophysiol*, 96, 3293-304.
- Horowitz, S. S., C. A. Cheney & J. A. Simmons (2004) Interaction of vestibular, echolocation, and visual modalities guiding flight by the big brown bat, *Eptesicus fuscus*. *J Vestib Res*, 14, 17-32.
- Hullar, T. E. & L. B. Minor (1999) High-frequency dynamics of regularly discharging canal afferents provide a linear signal for angular vestibuloocular reflexes. *J Neurophysiol*, 82, 2000-5.
- Lasker, D. M., G. C. Han, H. J. Park & L. B. Minor (2008) Rotational responses of vestibular-nerve afferents innervating the semicircular canals in the C57BL/6 mouse. *J Assoc Res Otolaryngol*, 9, 334-48.
- Li, A., J. Xue & E. H. Peterson (2008) Architecture of the mouse utricle: macular organization and hair bundle heights. *J Neurophysiol*, 99, 718-33.
- Lindeman, H. H. (1969) Regional differences in structure of the vestibular sensory regions. *J Laryngol Otol*, 83, 1-17.
- Lysakowski, A., S. Gaboyard-Niay, I. Calin-Jageman, S. Chatlani, S. D. Price & R. A. Eatock (2011) Molecular microdomains in a sensory terminal, the vestibular calyx ending. *J Neurosci*, 31, 10101-14.

- Lysakowski, A. & J. M. Goldberg (1997) A regional ultrastructural analysis of the cellular and synaptic architecture in the chinchilla cristae ampullares. *J Comp Neurol*, 389, 419-43.
- Lysakowski, A. & J. M. Goldberg (2008) Ultrastructural analysis of the cristae ampullares in the squirrel monkey (*Saimiri sciureus*). *J Comp Neurol*, 511, 47-64.
- Malinzak, M. D., R. F. Kay & T. E. Hullar (2012) Locomotor head movements and semicircular canal morphology in primates. *Proc Natl Acad Sci U S A*, 109, 17914-9.
- Meredith, F. L. & K. J. Rennie (2015) Zonal variations in K⁺ currents in vestibular crista calyx terminals. *J Neurophysiol*, 113, 264-76.
- Möhres, F. P. & E. Kulzer. 1956. Über die Orientierung der Flughund (*Chiroptera-Pteropodidae*). *Z. vergl. Physiol.* 38, 1-29.
- Ramprasad, F., J. P. Landolt, K. E. Money & J. Laufer (1980) Neuromorphometric features and dimensional analysis of the vestibular end organ in the little brown bat (*Myotis lucifugus*). *J Comp Neurol*, 192, 883-902.
- Riskin, D. K., J. Iriarte-Díaz, K. M. Middleton, K. S. Breuer & S. M. Swartz (2010) The effect of body size on the wing movements of pteropodid bats, with insights into thrust and lift production. *J Exp Biol*, 213, 4110-22.
- Sadeghi, S. G., M. J. Chacron, M. C. Taylor & K. E. Cullen (2007) Neural variability, detection thresholds, and information transmission in the vestibular system. *J Neurosci*, 27, 771-81.
- Spitzmaul, G., L. Tolosa, B. H. Winkelmann, M. Heidenreich, M. A. Frens, C. Chabbert, C. I. de Zeeuw & T. J. Jentsch (2013) Vestibular role of KCNQ4 and KCNQ5 K⁺ channels revealed by mouse models. *J Biol Chem*, 288, 9334-44.
- Spoor, F., T. Garland, G. Krovitz, T. M. Ryan, M. T. Silcox & A. Walker (2007) The primate semicircular canal system and locomotion. *Proc Natl Acad Sci U S A*, 104, 10808-12.
- Tong, B., A. J. Hornak, S. F. Maison, K. K. Ohlemiller, M. C. Liberman & D. D. Simmons (2016) Oncomodulin, an EF-Hand Ca²⁺ Buffer, Is Critical for Maintaining Cochlear Function in Mice. *J Neurosci*, 36, 1631-5.
- Yang, A. & T. E. Hullar (2007) Relationship of semicircular canal size to vestibular-nerve afferent sensitivity in mammals. *J Neurophysiol*, 98, 3197-205.
- Yovel, Y., B. Falk, C. F. Moss & N. Ulanovsky (2010) Optimal localization by pointing off axis. *Science*, 327, 701-4.